ACS APPLIED MATERIALS & INTERFACES

Research Article

www.acsami.org

Enhanced Air Stability of Polymer Solar Cells with a Nanofibril-Based Photoactive Layer

Jin Young Oh, Minkwan Shin, Hyun Woo Lee, Yu-Jeong Lee, Hong Koo Baik,* and Unyong Jeong*

Department of Materials Science and Engineering, Yonsei University, 134 Shinchong-dong, Seoul 120-750, Republic of Korea

Supporting Information

ABSTRACT: In spite of the rapid increase in the power conversion efficiency (PCE) of polymer solar cells (PSCs), the poor stability of the photoactive layer in air under sunlight is a critical problem blocking commercialization of PSCs. This study investigates the photo-oxidation behavior of a bulk-heterojunction (BHJ) photoactive film made of single-crystalline poly(3-hexlythiophene) (P3HT) nanofibrils and fullerene derivatives [phenyl-C_{61}-butyric methyl ester (PCBM), indene-C 60 bisadduct (ICBA)]. Because the single-crystalline P3HT nanofibrils had tightly packed $\pi-\pi$ stacking, the permeation of oxygen and water into the nanofibrils was significantly reduced. Chemical changes in P3HT were not apparent in the nanofibrils, and hence the air stability of the nanofibril-based BHJ film was considerably enhanced as compared with conventional BHJ films. The chemical changes were monitored by Fourier-transform infrared (FT-IR) spectroscopy, Raman spectroscopy, and UV−vis absorbance. Inverted PSCs made of the nanofibril-based BHJ layer also showed significantly enhanced air stability under sunlight. The nanofibril-based solar cell maintained more than 80% of its initial PCE after 30 days of continuous exposure to sunlight (AM 1.5G, 100 mW/cm^2), whereas the PCE of the conventional BHJ solar cell decreased to 20% of its initial PCE under the same experimental conditions.

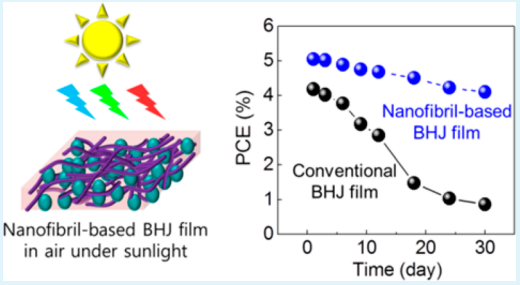

KEYWORDS: *polymer solar cells, nanofibrils, P3HT, crystallinity, air stability, photo-oxidation*

INTRODUCTION

Polymer solar cells (PSCs) based on polymer-donor and fullerene-acceptor bulk-heterojunction (BHJ) composites have received intensive attention because they are potentially inexpensive, mechanically flexible, lightweight, and adaptable to printed electronics.[1−3] PSCs with more than 10% power conversion efficiency (PCE), which has been regarded as the minimum efficiency needed to commercialize PSCs, have been achieved using low-band-gap polymers.[6−8] However, the instability of PSCs in air under sunlight is a critical problem that blocks their commercialization.[9] The stability remains a challenging issue to be solved in the near future.

The instability of PSCs in air originates from their corrosive electrode and photoactive materials, which are vulnerable to react with oxygen and water in air.[10−12] A number of methods have been introduced to increase the air stability of PSCs,[13−23] but failed to incresae it to the remarkable level such as those of inorganic-based solar cells or dye-sensitized solar cells. The most effective approach is replacing the oxidative electrode with an inert electrode, which is called the inverted structure in that the inert electrode is self-encapsulated.[24,25] This inverted structure is considered to be the proper device configuration for fabricating air-stable PSCs. However, the inherent instability of the photoactive materials, especially their vulnerability to photo-oxidation under sunlight in air, needs thorough study. Photo-oxidation occurs when a photoactive material is exposed to light in the presence of water or oxygen. The activated oxygen causes decomposition of the π-conjugation system of the light-absorbing molecules, which irreversibly degrades the PCE.[26−29] Consequently, various passivation layers are applied to prevent penetration of oxygen and water into the device.[30−32] However, these passivation layers cannot completely block the permeation of oxygen species from the outside, although the lifetime of the device is significantly enhanced through these efforts.[9,33,34] Thus, in terms of the materials used, fundamental approaches enhancing the stability of photoactive materials are required. Changing the chemical structure by a novel synthesis or optimizing the morphology of the photoactive polymers may be a possible means of accomplishing this.

Recently, nanofibril-based photoactive films using polythiophene-based donors have been introduced as an alternative morphology to conventional photoactive films consisting of randomly oriented nanocrystal donor and acceptor phases.[35−39] A nanofibril-based BHJ photoactive film provides a large donor/acceptor interfacial area and a well-interconnected current network. The structural advantage results in higher efficiency than is possible with conventional BHJ films. In addition, the nanofibril-based PSCs have shown robust properties in terms of thermal, mechanical stability.[35−37] The nanofibril-based photoactive films can be processed in air with no difference in PCE in devices prepared in an inert

Received: February 19, 2014
Accepted: April 1, 2014
Published: April 1, 2014

environment, demonstrating the enhanced air stability of the nanofibril-based films. However, studies on the air stability of nanofibril-based photoactive layers have not yet been reported.

In this study, we investigated the air stability of a photoactive film under sunlight, focusing on the polymer donor because it absorbs most of the photons in PSCs and determines the stability than the fullerene-based acceptor.[9,40−42] We used poly(3-hexylthiophene) (P3HT) as the polymer donor. Phenyl-C_{61}-butyric methyl ester (PCBM) and indene-C 60 bisadduct (ICBA) were used as the fullerene acceptor. We observed that the nanofibril-based BHJ photoactive films had a higher tolerance to photo-oxidation than the conventional BHJ photoactive film. Single-crystalline nanofibrils composed of closely packed $\pi-\pi$ stacking are relatively impermeable to oxygen species, and hence they reduced the photo-oxidation of P3HT. The nanofibril-based PSC maintained more than 80% of its initial PCE after 30 days, whereas the PCE of the conventional BHJ photoactive film decreased significantly to 20% after 30 days. The results suggest that remarkable improvement in the photo stability of the polymer can be obtained by generating crystalline nanofibrils. This approach improving the materials stability is a unique contribution distinct from the approaches focusing on passivation of the device.

EXPERIMENTAL SECTION

Preparation of Nanofibril-Based Photoactive Film. Poly(3-hexylthiophene) (P3HT, M_w = 50 000) with ∼95% regioregularity, phenyl-C61-butyric methyl ester (PCBM), and indene-C60 bisadduct (ICBA) were purchased from Reike Metal, Nano C, and Solarmer, respectively. The blended solutions (P3HT:PCBM and P3HT:ICBA = 1:1 w/w, 2 wt % in *m*-xylene) were cooled to −15 °C and then heated to room temperature in air, following the procedure previously reported by our group.[35−37] After this cycle of cooling and heating, the solution contained nanorod-like crystal seeds at room temperature. Long, uniform-sized nanofibrils were grown from the seed crystals during spin-coating, thus generating nanofibril-based photoactive BHJ films.

Sample Characterization. The morphology of the photoactive films was investigated by scanning electron microscopy (SEM, JSM-7001F, JEOL) and transmission electron microscopy (TEM, JEM-2011HC, JEOL). Chemical changes in the P3HT films after photo-aging were analyzed by Raman spectroscopy using a 532 nm green laser as the excitation source and infrared spectroscopy (Vertex 70 FT-IR spectrometer). The crystal structure of P3HT was measured by X-ray diffraction (XRD, Rigaku Ultima IV). The UV-vis absorbance spectra of the photoactive films were obtained by a Jasco V-570 spectrophotometer. All photoactive films were thermally annealied at 140 °C for 10 min to correspond with the condition of device fabrication before characterization.

Device Fabrication and Characterization. ITO-coated glass substates were sequentially cleaned in an ultrasonic bath of trichloroethylene, acetone, and isopropy alcohol. Then, the substrates were treated with UV/ozone for 30 min. A zinc oxide (ZnO) sol−gel solution was prepared by dissolving 7.4 M zinc acetate dihydrate and 8.1 M ethanoamine in 2-methoxyethanol by magnetic stirring at 80 °C for 1 h. The ZnO layer (30 nm) was prepared by spin-coating on the ITO glass and thermal annealing at 200 °C for 30 min. The blend solutions (P3HT:PCBM and P3HT:ICBA = 1:1 w/w, 2 wt % in *m*-xylene) were spin-coated on the ZnO-coated ITO glass. The thickness of the photoactive films was fixed at 150 nm. Subsequently, a thin film (40 nm) of poly(3,4-ethlylenedioxythiophene)-poly(styrenesulfonate) (PEDOT:PSS, Baytron P, Bayer AG) was spin-coated on the photoacive layer and the samples were annealed at 140 °C for 10 min in an N_2-filled glove box. Finally, a top electrode of Ag with an area of 5.4 mm^2 was deposited using thermal evaporation under high vacuum (1×10^{-6} Torr). The photovoltaic characteristics were measured using a Keithley 2400 instrument under 100 mW/cm^2 with AM 1.5G. An Oriel reference Si solar cell was used for calibration to ensure accurate measurements. The air stability of the device was tested as a function of time. For the dark environment, the devices were stored in a black acrylic box in ambient conditions (25 °C, 35% humidity in air). For the sunlight environment, the devices were exposed to 100 mW/cm^2 with AM 1.5G in air.

RESULTS AND DISCUSSION

Figure 1a shows a schematic illustration of our approach to fabricating a nanofibril-based photoactive film. The P3HT

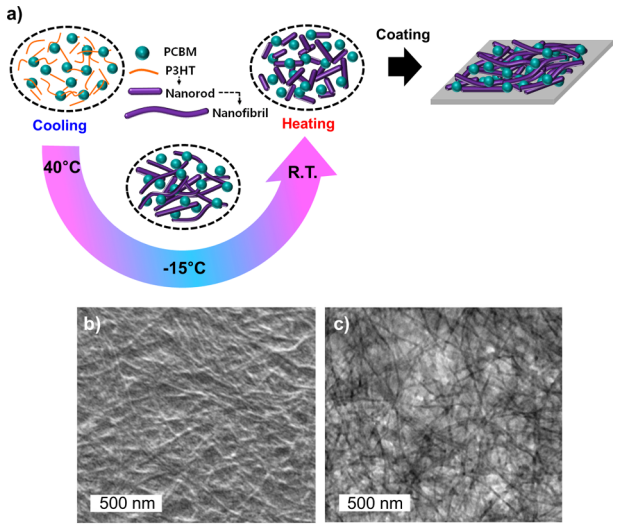

Figure 1. (a) Schematic illustration of the formation method of nanofibril-based photoactive film using a P3HT:PCBM solution subjected to cyclical cooling and heating (C&H). The P3HT nanorods formed after the C&H process quickly developed into single-crystal P3HT nanofibrils through self-seeded growth during the coating process. (b) SEM and (c) TEM images show the nanofibril-based photoactive film with a bicontinuous interpenetrating network of well-dispersed P3HT nanofibrils and PCBM molecules.

nanofibrils were generated by self-seeded growth, as we previously reported.[29] After a cycle of cooling to −15 °C and heating to room temperature, the P3HT:PCBM-blended xylene solution contained nanorod-like crystal seeds at room temperature. The seeds grew quickly during the coating process, which resulted in long (>10 μm) and thin (∼20 nm) P3HT nanofibrils. The SEM and TEM images shown in images b and c in Figure 1, respectively, show the morphology of the P3HT:PCBM BHJ photoactive layer.

To investigate the air stability of P3HT in the photoactive film under sunlight, we used Raman spectroscopy, which provided information about the changes in chemical structure caused by the photo-oxidation.[43−45] Figure 2a shows the Raman spectra of the conventional and nanofibril-based photoactive films with the same thickness (150 nm), which are annealed at 140 °C for 10 min before and after exposing the films for 10 h in air under sunlight (herein, we call the process "photo-aging"). The Raman spectra contain two strong vibrational modes related to the conjugation backbone of P3HT: the C═C symmetric stretching mode peak (∼1447 cm^{-1}) and the C−C stretching mode peak (∼1380 cm^{-1}) within the thiophene ring. The spectra provided information about the conjugation length and molecular order (crystallinity) of P3HT because the peaks are Raman-active due to

dx.doi.org/10.1021/am501034g | ACS Appl. Mater. Interfaces 2014, 6, 7759−7765

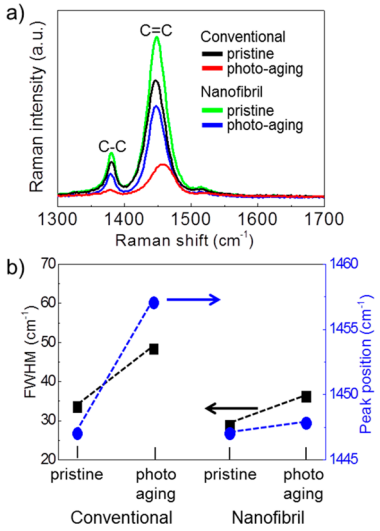

Figure 2. (a) Raman spectra of P3HT:PCBM photoactive films before and after the photo-aging process that exposed the film in air under sunlight for 10 h. (b) Full width at half maximum (FWHM and peak position of C═C mode of P3HT in photoactive film before and after photo-aging).

their strong coupling to the π electrons delocalized along the conjugated main backbone of the molecule. After photo-aging, the peak intensity and sharpness of the conventional BHJ film were reduced, and the C═C mode peak position shifted significantly to a higher wave number. The nanofibril-based BHJ film showed less of a decrease in the C═C mode peak intensity, and the peak position shifted slightly as compared to that in the conventional BHJ film. Figure 2b shows the changes of the peak position and full width at half maximum (FWHM) of the C═C mode peaks of both films before and after photo-aging. The results suggest that the nanofibril-based BHJ film has a higher tolerance to photo-oxidation than the conventional BHJ film. The drop of peak intensity indicates that the conjugate system of the P3HT molecule was destroyed. The large reduction of the C−S−C mode peak is evidence of the severe deformation of the P3HT thiophene ring in the conventional BHJ film, as shown in the Supporting Information, Figure S1. Also, the large shift of the conventional BHJ film's C═C mode peak to a higher wave number with a broad shape implies that the ordered (crystalline) P3HT phase changed to a disordered (amorphous) P3HT phase in the BHJ film. It indicates a critical correlation between the molecular deformation and crystallinity of the P3HT phase as a result of photo-aging.

To reveal the crystal percentage (crystallinity) and the P3HT morphology, the crystallinity of P3HT in photoactive films was measured with differential scanning calorimetry (DSC). Figure 3 shows the DSC thermograms of the conventional BHJ film and the nanofibril-based BHJ film, and their corresponding photo-aged films under sunlight for 10 h. The crystallinity was calculated using DSC melting peak (210−240 °C),[46,47] $X_C = \Delta H_m / (\Delta H_f \cdot \phi_{P3HT}) \times 100$ %, where X_C is crystallinity of polymer, ΔH_m is the melting enthalpy of crystalline polymer, ΔH_f is the melting enthalpy of 100 % crystalline polymer, and ϕ_{P3HT} (0.5) is weight fraction of P3HT. The ΔH_f of P3HT was reported recently to be 37 J/g.[48] The ΔH_m of the conventional BHJ film was 11.90 J/g; hence X_C was 59.94 %. The ΔH_m of the nanofibril-based BHJ film was 18.32 J/g; hence X_C was 99.02 %, which indicates that the nanofibril-based photoactive

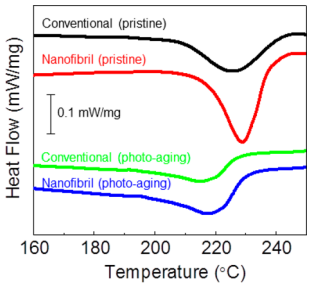

Figure 3. DSC heat flow of the photoactive films; conventional BHJ film (black) and the corresponding film after photo-aging (green), nanofibril-based film (red), and the corresponding film after photo-aging (blue).

film is composed of nearly 100% crystalline P3HT. After photo-aging, the ΔH_m of the conventional film decreased to 6.10 J/g (so, X_C = 32.97 %) and the ΔH_m of the nanofibril-based film showed smaller decrease to 12.42 J/g (so, X_C = 67.13 %). These results indicate that the photo-aging damages the crystal structure and decreases the crystallinity.

Another means to correlate the crystallinity and photoagain is XRD analysis. We compared four different types of photoactive film: the nanofibril-based BHJ film (1) before and (2) after photo-aging, and the conventional BHJ film (3) before and (4) after photo-aging. The photoactive films were annealed at 140 °C for 10 min. The results are shown in Figure 4. The peak at 2θ = 5−6° represents the (100) plane of the

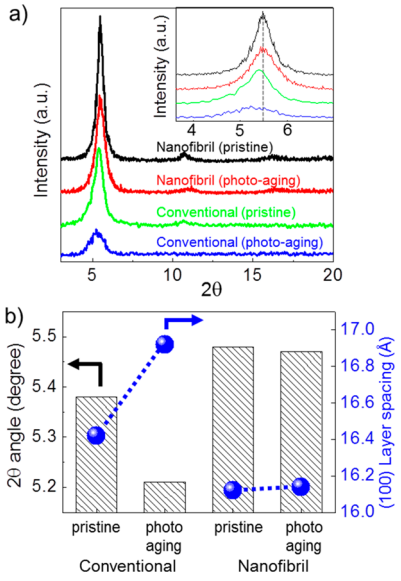

Figure 4. (a) Out-of-plane X-ray diffraction (XRD) of P3HT:PCBM photoactive films before and after photo-aging. (b) Change in the 2θ angle and the interlayer spacing of the (100) plane of the photoactive films before and after photo-aging.

$\pi-\pi$ stacking of P3HT, and the peaks at 2θ = 10−11° and 16−17° represent the (200) and (300) planes, respectively. As previously reported, the nanofibril-based photoactive layer showed a higher peak intensity with a narrower FWHM than the conventional BHJ film (Supporting Information, Figure S2).[35−39] The crystallinity of the conventional BHJ film significantly decreased with a large FWHM after photo-aging, whereas the nanofibril-based film showed less decline of P3HT crystallinity.

dx.doi.org/10.1021/am501034g | ACS Appl. Mater. Interfaces 2014, 6, 7759−7765

For further insight into the effect of the crystallinity on the molecular deformation of P3HT by photo-oxidation, the chemical structure of P3HT was investigated by fast Fourier-transform infrared spectroscopy (FT-IR). Figures 5a and b

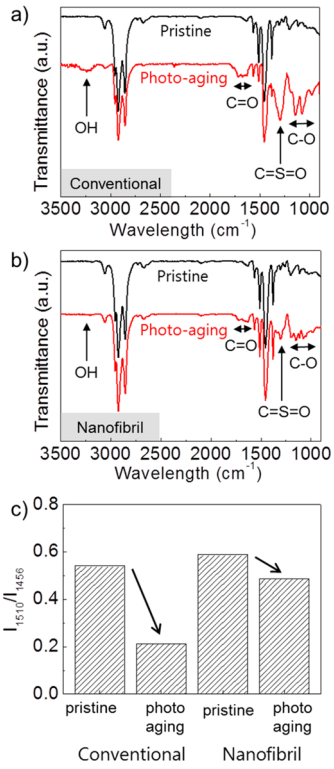

Figure 5. FT-IR spectra of (a) conventional P3HT film and (b) nanofibril-based P3HT film before and after photo-aging. (c) Change of I_{1510}/I_{1456} ratio of the P3HT films, which represents the average effective conjugation length of P3HT.

show FT-IR spectra of the conventional and nanofibril-based P3HT films, respectively, before and after photo-aging. In the conventional P3HT film after photo-aging, oxygen-containing moieties such as C═O (1710 and 1685 cm^{-1}), C═S═C (1253 cm^{-1}), and C−O (1200−1100 cm^{-1}) were clearly observed in the FT-IR spectra. In the nanofibril-based P3HT after photo-aging, peaks corresponding to oxygen-containing moieties were not apparent. The hydroxyl group peak (−OH, ~3200 cm^{-1}) was not detectable in the conventional P3HT film. The intensity ratio of the asymmetric C═C stretching mode peak at 1510 cm^{-1} (I_{1510}) and the symmetric ring stretching mode peak at 1456 cm^{-1} (I_{1456}) was used to compare the average effective conjugation length of P3HT.[49−51] Figure 5c shows the I_{1510}/I_{1456} peak ratios of both P3HT films before and after photo-aging. The peak ratio (I_{1510}/I_{1456}) of the conventional P3HT film decreased considerably after photo-aging, whereas the nanofibril-based P3HT film exhibited only a slight decrease.

These molecular change caused by photo-aging is significantly affected by the crystal structure of P3HT. Scheme 1 shows the possible two routes of the reaction that were proposed in the previous literatures.[10,40,52−54] The activated oxygens react with sp^2 bonds and generate sp^3 bonds with hydroxyl groups and carbonyl groups (Scheme 1a),[10,52] or they form ether first and detach the grafted hexyl groups (Scheme 1B).[40,53,54] The $sp^2 \rightarrow sp^3$ transformation causes deformation

Scheme 1. Possible Reaction Schemes for Photo Oxidation of P3HT; (a) Reaction Mechanism Suggested in Refs 10, 52; (b) Reaction Mechanism Suggested in Refs 40, 53, 54

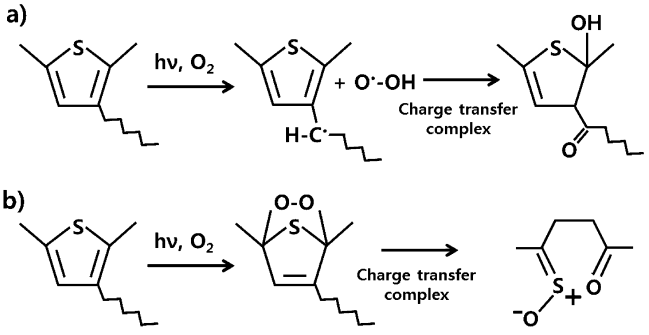

of the crystal structure. This degradation of the π-conjugation becomes prominent when the concentration of the oxygen species in the P3HT film is high and the interlayer packing by the $\pi-\pi$ conjugation is loose. The penetration of oxygen species takes place mainly through the amorphous region of P3HT and the grain boundaries; hence the conventional thin films are vulnerable to the oxidation due to the larger fraction of amorphous P3HT and the large number of grain boundaries between the nanoscale crystal grains. The completeness of the $\pi-\pi$ stacking may be compared by the sharpness of the XRD peak corresponding to (100) and the interlayer spacing. The sharp XRD peak and the smaller interlayer spacing of the nanofibrils indicate that the conjugated layers are more closely packed and the persistence length of the stacking along [100] is long. In contrast, the conventional thin film has a broad low XRD intensity (large FWHM) from (100) plane and the interlayer spacing is slightly larger, which indicates a loose crystal packing and a short persistence length of the stacking along [100]. The structural change from sp^2 to sp^3 bonding requires more space. The tight packing and long persistence length in the nanofibrils can play as an energetic barrier for the structural change of the polymer chains; meanwhile the loose, defected interlayer packing in the conventional film cannot. Therefore, the P3HT nanofibril provides enhanced stability than the conventional films do.

Such chemical degradation affects the optical properties because the photon absorbance of a molecule depends on its chemical structure and crystallinity. Panels a and b in Figure 6 show the UV−vis absorption spectra of the conventional and nanofibril-based BHJ films, respectively, before and after photo-aging. The UV−vis spectra of the conventional photoactive film showed a substantial reduction of photon absorption of P3HT, with a large blue-shift of the main peak. The shoulder peaks (~550 and ~605 nm) indicating the intensity of $\pi-\pi$ interaction of the thiophene ring disappeared, which supports the claim that the π-conjugation system of the P3HT molecular chain and the degree of $\pi-\pi$ stacking was severely destroyed by photo-oxidation. In contrast, the nanofibril-based photoactive film exhibited only a slight reduction of photon absorption while maintaining the original shape of the P3HT absorption peak.

To verify the air stability of the nanofibril-based BHJ film under sunlight, we fabricated inverted PSCs with sequential layers of ITO/ZnO/P3HT:PCBM/PEDOT:PSS/Ag. The air-stability tests of the photoactive films were conducted prior to deposition of the anode layer (PEDOT:PSS/Ag) because the sunlight (100 mW/cm^2 with AM 1.5G) directly affects the

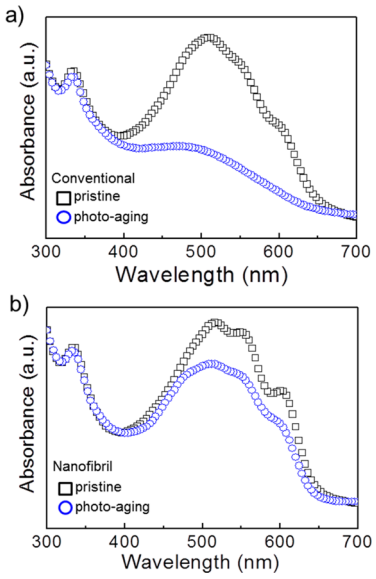

Figure 6. UV−vis absorption spectra of (a) the conventional BHJ film and (b) the nanofibril-based BHJ film before and after photo-aging.

photoactive film in air, which clarifies air stability of photoactive film compared to the photoactive film covered by electrode, as shown in Scheme 2.

Scheme 2. Schematic Illustration of a Strategy to Exam the Air Stability of the Photoactive Film by Directly Exposing the Photoactive Film on the ZnO-Deposited ITO-Glass under Sunlight in Air with an Average Humidity of 35%[a]

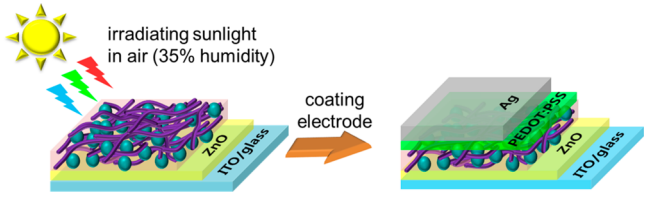

[a]We evaluated the properties of the photoactive film in terms of its photovoltaic performance after the deposition of PEDOT:PSS and a Ag electrode.

The results of the stability tests of the photoactive films in the devices are represented in Figure 7. Panels a and b in Figure 7 show representative photocurrent density−voltage (J−V) curves, and Figure 7c−f exhibit the photovoltaic parameters of the devices. The values are summarized in the Supporting Information, Tables S1 and S2. The PCE of the device with the conventional photoactive layer decreased significantly from 3.04 to 0.55% (18% of its initial PCE) after exposing the photoactive layer to sunlight for 10 h in air. The main causes of the degraded performance were the short-circuit current density (J_{sc}) and fill factor (FF), which are related to photon absorption and carrier transport. The oxygen-containing moieties resulting from photo-aging act as defects and trap sites. The degraded conjugation reduces the current path in the photoactive film. However, the device with the nanofibril-based photoactive layer exhibited much more stable photovoltaic performance under the same conditions. The PCE of the device with the nanofibril-based photoactive film was 1.95% after photo- aging for 10 h (53.6% of the initial PCE of 3.65%). Again, the major reasons for the PCE reduction were decreases

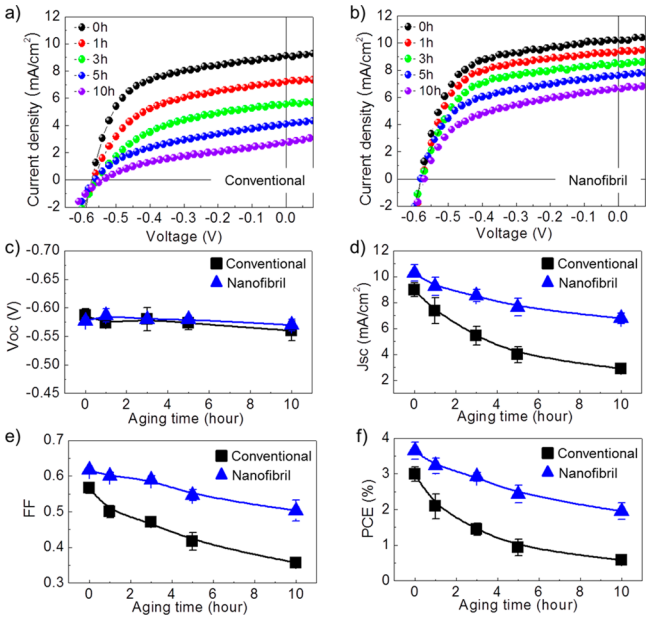

Figure 7. Representative J−V curves of PSCs with (a) the conventional photoactive film and (b) the nanofibril-based photoactive film as a function of photo-aging time before deposition of PEDOT:PSS/Ag electrode. Influence of the type of photoactive film on the (c) V_{oc}, (d) J_{sc}, (e) FF, and (f) PCE of the solar cells.

of J_{sc} and FF by photo-oxidation. This photovoltaic performance corresponds to the observation that the nanofibril-based photoactive film has better tolerance to photo-oxidation than the conventional photoactive film. The single-crystalline nanofibril-based photoactive film may therefore be a promising candidate for air-stable photovoltaic devices.

To further explore the feasibility of high efficiency, air-stable P3HT nanofibril-based photoactive films, we tested another frequently studied BHJ system using indene-C60 bisadduct (ICBA). ICBA was recently introduced as an alternative to PCBM acceptors because the P3HT:ICBA system has a larger gap between the highest occupied molecular orbital (HOMO) of the polymer donor and the lowest unoccupied molecular orbital (LUMO) of the ICBA acceptor than the P3HT:PCBM system.[55−57] Figure 8a shows the J−V curves of the solar cells made of the P3HT:ICBA BHJ films. The device with the nanofibril-based photoactive film showed higher efficiency (5.123%) than the device with a conventional photoactive layer (4.202%). The photovoltaic parameters of both devices are summarized in Table S3 in the Supporting Information. Figure 8b exhibits the change in PCE of the solar cells made with the conventional P3HT:ICBA photoactive film and that of the P3HT nanofibril:ICBA photoactive film as a function of time. To investigate the actual effect of photo-oxidation in air under sunlight, we prepared a pair of the same devices and stored one of them in the dark in air and the other under 100 mW/cm^2 with AM 1.5G in air. The specific details of the air-stability test are described in the Experimental Section. The efficiency of the device made of the conventional film decreased significantly under sunlight after 3 days and remained at 20% of its initial PCE after 30 days. The device stored in the dark remained at approximately 80% of its initial PCE after 30 days, which indicates that the reduction of efficiency was caused by photo-oxidation under sunlight. In contrast, the nanofibril-based PSC maintained more than 80% of its initial PCE under sunlight even after 30 days. Its stability was also better in the

dx.doi.org/10.1021/am501034g | ACS Appl. Mater. Interfaces 2014, 6, 7759−7765

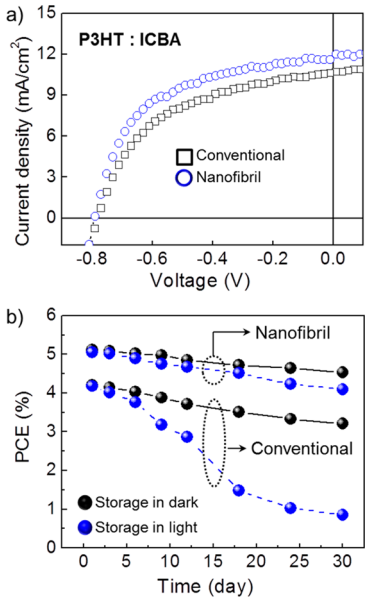

Figure 8. (a) Representative *J*–*V* curves of PSCs with P3HT:ICBA BHJ film as a function of its BHJ film type. (b) Changes in PCE of a PSC with a conventional photoactive film and a PSC with a nanofibril-based photoactive film according to the storage type of the device in air with an average humidity of 35%.

dark, maintaining 92% of its initial PCE. These results clearly prove that the nanofibril-based photoactive film is superior to conventional photoactive films in terms of photo-oxidation in air.

CONCLUSION

We investigated the photo-oxidation behavior of photoactive films consisting of single-crystalline P3HT nanofibrils and fullerene derivatives (PCBM or ICBA). Single-crystalline P3HT nanofibrils having tightly packed π–π stacking were much less permeable to oxygen species, and hence the chemical degradation of P3HT by photo-oxidation in air could be delayed considerably as compared with conventional photoactive films. On the basis of these results, we fabricated inverted solar cells made of the two types of photoactive film and examined the air stability of the devices. The power conversion efficiency (PCE) of the device made of the nanofibril-based photoactive film maintained more than 80% of its initial PCE after 30 days, whereas the PCE of the device made of the conventional photoactive film decreased significantly to 20% of its initial value after 30 days. These results clearly demonstrate that the nanofibril-based photoactive film is promising for producing air-stable polymer solar cells with high efficiency.

ASSOCIATED CONTENT

Supporting Information

Tables of the photovoltaic properties, Raman spectroscopy of the photoactive layers, analysis of XRD data. This material is available free of charge via the Internet at http://pubs.acs.org.

AUTHOR INFORMATION

Corresponding Author

*E-mail: ujeong@yonsei.ac.kr, thinfilm@yonsei.ac.kr.

Notes

The authors declare no competing financial interest.

ACKNOWLEDGMENTS

This work was supported by a grant from the National Research Foundation of Korea (NRF) (2012-0008721 and 2011-0022765) funded by the Korean government (MEST). U.J. acknowledges the financial support by MEST through the Active Polymer Center Pattern Integration (R11-2007-050-01004-0).

REFERENCES

(1) Wöhrle, D.; Meissner, D. Organic Solar Cells. *Adv. Mater.* **1991**, *3*, 129–138.
(2) Li, G.; Zhu, R.; Yang, Y. Polymer Solar Cells. *Nat. Photonics* **2012**, *6*, 153–161.
(3) Ameri, T.; Li, N.; Brabec, C. J. Highly Efficient Organic Tandem Solar Cells: A Follow up Review. *Energy Environ. Sci.* **2013**, *6*, 2390–2413.
(4) Dou, L.; You, J.; Hong, Z.; Xu, Z.; Li, G.; Street, R. A.; Yang, Y. A Decade of Organic/Polymeric Photovoltaic Research. *Adv. Mater.* **2013**, *25*, 6642–6671.
(5) Jørgense, M.; Norrman, K.; Gevorgyan, S. A.; Tromholt, T.; Andreasen, B.; Krebs, F. C. Stability of Polymer Solar Cells. *Adv. Mater.* **2012**, *24*, 580–612.
(6) www.heliateck.eu. *Heliatek reported new world record for organic solar cell with certified 12.0 % cell efficiency.*
(7) You, J.; Dou, L.; Yoshimura, K.; Kato, T.; Kenichrio, O.; Moriarty, T.; Emery, K.; Chen, C.-C.; Gao, J.; Li, G.; Yang, Y. A Polymer Tandem Solar Cell with 10.6% Power Conversion Efficiency. *Nat. Commun.* **2013**, *4*, 1446.
(8) Dennler, G.; Scharber, M. C.; Ameri, T.; Denk, P.; Forberich, K.; Waldauf, C.; Brabec, C. J. Design Rules for Donors in Bulk-Heterojunction Tandem Solar Cells-Towards 15 % Energy-Conversion Efficiency. *Adv. Mater.* **2008**, *20*, 579–583.
(9) Lee, J. U.; Jung, J. W.; Jo, J. W.; Jo, W. H. Degradation and Stability of Polymer-Based Solar Cells. *J. Mater. Chem.* **2012**, *22*, 24265–24283.
(10) Jørgense, M.; Norrman, K.; Kebs, F. C. Stability/Degradation of Polymer Solar Cells. *Sol. Energy Mater. Sol. Cells* **2008**, *92*, 686–714.
(11) Kawano, K.; Pacios, R.; Poplavskyy, D.; Nelson, J.; Bradley, D. D. C.; Durrant, J. R. Degradation of Organic Solar Cells Due to Air Exposure. *Sol. Energy Mater. Sol. Cells* **2006**, *90*, 3520–3530.
(12) Norrman, K.; Gevorgyan, S. A.; Krebs, F. C. Water-Induced Degradation of Polymer Solar Cells Studied by $H_2{}^{18}O$ Labeling. *ACS Appl. Mater. Interfaces* **2009**, *1*, 102–112.
(13) Hsieh, C.-H.; Cheng, Y.-J.; Li, P.-J.; Chen, C.-H.; Dubosc, M.; Liang, R.-M.; Hsu, C.-S. Highly Efficient and Stable Inverted Polymer Solar Cells Integrated with a Cross-Linked Fullerene Material as an Interlayer. *J. Am. Chem. Soc.* **2010**, *132*, 4887–4893.
(14) Lee, K.; Kim, J. Y.; Park, S. H.; Kim, S. H.; Cho, S.; Heeger, A. J. Air-Stable Polymer Electronic Devices. *Adv. Mater.* **2007**, *19*, 2445–2449.
(15) Krebs, F. C.; Spanggaard, H. Significant Improvement of Polymer Solar Cell Stability. *Chem. Mater.* **2005**, *17*, 5235–5237.
(16) Sun, Y.; Takacs, C. J.; Cowan, S. R.; Seo, J. H.; Gong, X.; Roy, A.; Heeger, A. J. Efficient, Air-Stable Bulk Heterojunction Polymer Solar Cells Using MoO_x as the Anode Interfacial Layer. *Adv. Mater.* **2011**, *23*, 2226–2230.
(17) Khelifi, S.; Voroshazi, E.; Spoltore, D.; Piersimoni, F.; Bertho, S.; Aernouts, T.; Manca, J.; Lauwaert, J.; Vrielinck, H.; Burgelman, M. Effect of Light Induced Degradation on Electrical Transport and Charge Extraction in Polythiophene:Fullerene (P3HT:PCBM) Solar Cells. *Sol. Energy Mater. Sol. Cells* **2014**, *120*, 244–252.
(18) Seemann, A.; Egelhaaf, H.-J.; Brabec, C. J.; Hauch, J. A. Influence of Oxygen on Semi-Transparent Organic Solar Cells with Gas Permeable Electrodes. *Org. Electron.* **2009**, *10*, 1424–1428.
(19) Wang, Q.; Aziz, H. Poor Photo-Stability of the Organic/LiF/Al Contact in Organic Optoelectronic Devices. *Org. Electron.* **2011**, *12*, 1571–1575.

(20) Shin, W. H.; Park, S.-Y.; Park, M. Y.; Seo, H. O.; Kim, K.-D.; Kim, K.-D.; Kim, Y. T.; Kim, Y. D.; Kang, J.-W.; Lee, K. H.; Jeong, Y.; Kim, Y. D.; Lim, D. C. Multifunctional SWCNT-ZnO Nanocomposites for Enhancing Performance and Stability of Organic Solar Cells. *Adv. Mater.* **2011**, *23*, 519−522.
(21) Kim, C. S.; Kim, J. B.; Lee, S. S.; Kim, Y. S.; Loo, Y.-L. Sequence of Annealing Polymer Photoactive Layer Influences the Air Stability of Inverted Solar Cells. *Org. Electron.* **2009**, *10*, 1483−1488.
(22) Lin, C.; Lin, E.-Y.; Tsai, F.-Y. Enhanced Thermal Stability and Efficiency of Polymer Bulk-Heterojunction Solar Cells by Low-Temperature Drying of the Active Layer. *Adv. Funct. Mater.* **2010**, *20*, 834−839.
(23) Li, C.-Y.; Wen, T.-C.; Lee, T.-H.; Guo, T.-F.; Huang, J.-C.-A. An Inverted Polymer Photovoltaic Cell with Increased Air Stability Obtained by Employing Novel Hole/Electron Collecting Layers. *J. Mater. Chem.* **2009**, *19*, 1643−1647.
(24) Hau, S. K.; Yip, H.-L.; Beak, N. S.; Zou, J.; O'Malley, K. High Performance Ambient Processed Inverted Polymer Solar Cells through Interfacial Modification with a Fullerene Self-Assembled Monolayer. *Appl. Phys. Lett.* **2008**, *92*, 253301.
(25) Zimmermann, B.; Würfel, U.; Niggemann, M. Longterm Stability of Efficient Inverted P3HT:PCBM Solar Cells. *Sol. Energy Mater. Sol. Cells* **2009**, *93*, 491−496.
(26) Pacios, R.; Chatten, A. J.; Kawano, K.; Durrant, J. R.; Bradley, D. D. C.; Nelson, J. Effects of Photo-oxidation on the Performance of Poly[2-methoxy-5-(3′,7′-dimethyloctyloxy)-1,4-phenylene vinylene]: [6,6]-Phenyl C61-Butyric Acid Methyl Ester Solar Cells. *Adv. Funct. Mater.* **2006**, *16*, 2117−2126.
(27) Rivaton, A.; Chambon, S.; Manceau, M.; Gradette, J.-L.; Lemaître, N.; Guillerez, S. Light-Induced Degradation of the Active Layer of Polymer-Based Solar Cells. *Polym. Degrad. Stab.* **2010**, *95*, 278−284.
(28) Cook, S.; Furube, A.; Katoh, R. Matter of Minutes Degradation of Poly(3-hexylthiophene) under Illumination in Air. *J. Mater. Chem.* **2013**, *22*, 4282−4289.
(29) Günes, S.; Neugebauer, H.; Saricifitci, N. S. Conjugated Polymer-Based Organic Solar Cells. *Chem. Rev.* **2007**, *107*, 1324−1338.
(30) Dennler, G.; Lungenschmied, C.; Neugebauer, H.; Sariciftci, N. S.; Latrèche, M.; Czeremuszkin, G.; Wertheimer, M. R. A New Encapsulation Solution for Flexible Organic Solar Cells. *Thin Solid Films* **2006**, *511*, 349−353.
(31) Potscavage, W. J.; Yoo, S.; Domercq, B.; Kippelen, B. Encapsulation of Pentacene/C_{60} Organic Solar Cells with Al_2O_3 Deposited by Atomic Layer Deposition. *Appl. Phys. Lett.* **2007**, *90*, 253511.
(32) Krebs, F. C. Encapsulation of Polymer Photovoltaic Prototypes. *Sol. Energy Mater. Sol. Cells* **2006**, *90*, 3633−3643.
(33) Krebs, F. C.; Gevorgvan, S. A.; Alstrup, J. A Roll-to-Roll Process to Flexible Polymer Solar Cells: Model Studies, Manufacture and Operational Stability Studies. *J. Mater. Chem.* **2009**, *19*, 5442−5451.
(34) Lungenschmied, C.; Dennler, G.; Neugebauer, H.; Saricitci, S. N.; Glatthaar, M.; Meyer, T. *Sol. Energy Mater. Sol. Cells* **2007**, *91*, 379−384.
(35) Oh, J. Y.; Shin, M.; Lee, T. I.; Jang, W. S.; Min, Y.; Myoung, J.-M.; Baik, H. K.; Jeong, U. Self-Seeded Growth of Poly(3-hexylthiophene) (P3HT) Nanofibrils by a Cycle of Cooling and Heating in Solutions. *Macromolecules* **2012**, *45*, 7504−7513.
(36) Oh, J. Y.; Shin, M.; Lee, T. I.; Jang, W. S.; Lee, Y.-J.; Kim, C. S.; Kang, J. W.; Myoung, J.-M.; Baik, H. K.; Jeong, U. Highly Bendable Large-Area Printed Bulk Heterojunction Film Prepared by the Self-Seeded Growth of poly(3-hexylthiophene) Nanofibrils. *Macromolecules* **2013**, *46*, 3534−3543.
(37) Oh, J. Y.; Lee, T. I.; Jang, W. S.; Chae, S. S.; Park, J. H.; Lee, H. W.; Myoung, J.-M.; Baik, H. K. Mass Production of a 3D Non-Woven Nanofabric with Crystalline P3HT Nanofibrils for Organic Solar Cells. *Energy Environ. Sci.* **2013**, *6*, 910−917.
(38) Kim, J. S.; Lee, J. H.; Park, J. H.; Shim, C.; Sim, M.; Cho, K. High-Efficiency Organic Solar Cells Based on Preformed poly(3-hexylthiophene) Nanowires. *Adv. Funct. Mater.* **2011**, *21*, 480−486.
(39) Berson, S.; Bettignies, E. D.; Bailly, S.; Guillerez, S. Poly(3-hexylthiophene) Fibers for Photovoltaic Applications. *Adv. Funct. Mater.* **2007**, *17*, 1377−1384.
(40) Hintz, H.; Egelhaaf, H.-J.; Lüer, L.; Hauch, J.; Peisert, H.; Chassé, T. Photodegradation of P3HT-A Systematic Study of Environmental Factors. *Chem. Mater.* **2011**, *23*, 145−154.
(41) Neugebauer, H.; Brabec, C.; Hummelen, J. C.; Saricifci, N. S. Stability and Photodegradation Mechanisms of Conjugated Polymer/Fullerene Plastic Solar Cells. *Sol. Energy Mater. Sol. Cells* **2000**, *61*, 35−42.
(42) Thompson, B. C.; Fréchet, M. J. Polymer−Fullerene Composite Solar Cells. *Angew. Chem., Int. Ed.* **2008**, *47*, 58−77.
(43) Tsoi, W. C.; James, D. T.; Kim, J. S.; Nicholson, P. G.; Murphy, C. E.; Bradley, D. D. C.; Nelson, J.; Kim, J.-S. The Nature of In-Plane Skeleton Raman Modes of P3HT and Their Correlation to the Degree of Molecular Order in P3HT:PCBM Blend Thin Films. *J. Am. Chem. Soc.* **2011**, *133*, 9834−9843.
(44) Razzell-Hollis, J.; Tsoi, W. C.; Kim, J.-S. Directly Probing the Molecular Order of Conjugated Polymer in OPV Blends Induced by Different Film Thicknesses, Substrates and Additives. *J. Mater. Chem. C* **2013**, *1*, 6235−6243.
(45) Motaung, D. E.; Malgas, G. F.; Arendse, C. J. Insights into the Stability and Thermal Degradation of P3HT:C_{60} Blended Films for Solar Cell Applications. *J. Mater. Sci.* **2011**, *46*, 4942−4953.
(46) Van Krevelen, D. W. *Properties of Polymers*, 3rd ed.; Elsevier: Amsterdam, 1990.
(47) Abu-Zahra, N.; Algazzar, M. Effect of Crystallinity on the Performance of P3HT/PC70BM/n-Dodecylthiol Polymer Solar Cells. *J. Sol. Energy Eng.* **2013**, *136*, 021023.
(48) Pascui, O. F.; Lohwasser, R.; Sommer, M.; Thelakkat, M.; Thurn-Albrecht, T.; Saalwächter, K. High Crystallinity and Nature of Crystal−Crystal Phase Transformations in Regioregular Poly(3-hexylthiophene). *Macromolecules* **2010**, *43*, 9401−9410.
(49) Trznadel, M.; Pron, A.; Zagorska, M.; Chrzaszcz, R.; Pielichowski, J. Effect of Molecular Weight on Spectroscopic and Spectroelectrochemical Properties of Regioregular Poly(3-hexylthiophene). *Macromolecules* **1998**, *31*, 5051−5058.
(50) Motaung, D. E.; Malgas, G. F.; Arendse, C. J.; Mavundla, S. E.; Knoesen, D. Structural and Photo-Physical Properties of Spin-Coated Poly (3-hexylthiophene) Thin Films. *Mater. Chem. Phys.* **2009**, *116*, 279−283.
(51) Chang, Y.-M.; Su, W.-F.; Wang, L. Influence of Photo-Induced Degradation on the Optoelectronic Properties of Regioregular poly(3-hexylthiophene). *Sol. Energy Mater. Sol. Cells* **2008**, *92*, 761−765.
(52) Matturro, M.G.; Reynolds, R.P.; Kastrup, R.V.; Pictroski, C.F. Thioozonide Decomposition. Sulfur and Oxygen Atom Transfer. Evidence for the Formation of a Carbonyl O-Sulfide Intermediate. *J. Am. Chem. Soc.* **1986**, *108*, 2775−2776.
(53) Aguirre, A.; Meskers, S. C. J.; Janssen, R. A. J.; Egelhaaf, H.-J. Formation of Metastable Charges as a First Step in Photoinduced Degradation in π-Conjugated Polymer:Fullerene Blends for Photovoltaic Applications. *Org. Electron.* **2011**, *12*, 1657−1662.
(54) Hintz, H.; Egelhaaf, H.-J.; Peisert, H.; Chassé, T. Photo-Oxidation and Ozonization of Poly(3-hexylthiophene) Thin Films as Studied by UV/VIS and Photoelectron Spectroscopy. *Polym. Degrad. Stab.* **2010**, *95*, 818−824.
(55) He, Y.; Chen, H.-Y.; Hou, J.; Li, Y. Indene−C60 Bisadduct: A New Acceptor for High-Performance Polymer Solar Cells. *J. Am. Chem. Soc.* **2010**, *132*, 1377−1382.
(56) Li, H.; Li, Y.-F.; Wang, J. Optimizing Performance of Layer-by-Layer Processed Polymer Solar Cells. *Appl. Phys. Lett.* **2012**, *101*, 033907.
(57) Zhao, G.; He, Y.; Li, Y. 6.5% Efficiency of Polymer Solar Cells Based on poly(3-hexylthiophene) and Indene-C_{60} Bisadduct by Device Optimization. *Adv. Mater.* **2010**, *22*, 4355−4358.